XANES Characterization of Extremely Nanosized Metal-Carbonyl Subspecies (Me = Cr, Mn, Fe, and Co) Confined into the Mesopores of MCM-41 Materials

José M. Ramallo-López,[†] Eduardo J. Lede,[†] Félix G. Requejo,*[,†] José A. Rodriguez,[‡] Jae-Y. Kim,[‡] Raúl Rosas-Salas,[§] and José M. Domínguez*[,§]

Dto. Física, FCE, UNLP and IFLP (CONICET), P.O. BOX 67, 1900 La Plata, Argentina, Chemistry Department, Brookhaven National Laboratory, Upton, New York 11973, and Instituto Mexicano del Petróleo, Programa de Ingeniería Molecular, Eje Central Lázaro Cárdenas 152, 07730, México D. F.

Received: February 19, 2004; In Final Form: August 11, 2004

A study of the stability, local order, and interaction of the surface silanol groups of MCM-41 with transition metal carbonyls $M_x(CO)_y$ (where M = Cr, Mn, Fe, Co) introduced by a chemical alternative method was performed by X-ray absorption near-edge spectroscopy (XANES). These molecular species, catalytically active for ethylene polymerization reactions, were previously characterized by FTIR and NMR in order to confirm their monodispersion and confined location into the mesopores of the MCM-41 material. Present experimental results indicate the high dispersion of metal species in all cases. Symmetry and stability depend on type of compound, Fe-carbonyl having the lowest stability. Changes in metal coordination and oxidation state are clearly followed by XANES indicating the interaction between sub-carbonyl species and the walls of the mesopores.

Introduction

Nanostructures of metals or metal oxides confined inside mesoporous materials are important due to their potential applications in many areas of physics, chemistry, and materials science. The honeycomblike structure of mesoporous MCM-41 molecular sieves is constituted by a hexagonal array of uniform pores[1,2] having diameters four to five times larger than wide-pore zeolites such as Beta, Mazzite, or HY.[3,4] Unlike zeolites, the partial substitution of Si^{4+} framework atoms by Al^{3+} in MCM-41 materials leads to a milder surface acidity and a lower hydrothermal stability,[5,6] but these properties are being investigated and improved with the purpose of developing potential applications in catalysis, hydrogen mass storage media, adsorption, and separation technologies.[7,8] Recent developments report higher structural stability of a series of mesoporous materials based on MCM-41,[9] SBA-15,[10] MSU, and other structures,[11] according to the conditions prevailing during the synthesis or by means of postsynthesis treatments. Thus, there is a potential outcome toward the application of these materials in industry, especially for the fabrication of electromagnetic devices and for carrying out reactions involving bulky molecules from renewable sources or heavy oil feedstock. As those catalytic properties depend on specific active site arrays, the present investigation focused on creating the confined active groups into the pore space of MCM-41 from $M_x(CO)_y$ (M = Cr, Mn, Fe, Co) species, which were anchored to the glassy-like walls conforming the 1-D channels. These systems can be used as a nanometric reactor, which has been found to possess superior catalytic activity during ethylene polymerization reactions compared to conventional homogeneous carbonyl-based catalysts.[12]

* Corresponding authors. E-mail (Requejo): requejo@fisica.unlp.edu.ar. E-mail (Domínguez): jmdoming@imp.mx.
[†] Dto. Física, FCE, UNLP and IFLP (CONICET).
[‡] Brookhaven National Laboratory.
[§] Instituto Mexicano del Petróleo.

For the purpose of determining the local structure and electronic characteristics of transition metal species confined in the mesopores of the MCM-41 material, XANES emerges as an especially appropriate technique. In effect, being that XANES is associated with the structure of the absorption of X-rays related to electronic transitions from deep levels to unoccupied ones around the ionization potential (IP) of the atom, the extracted information is very sensitive to the chemical environment (such as site symmetry and oxidation state).

The 1s edges of the 3d transition metals have absorption edges for photon energies ranging from about 4 to 9 keV. Their XANES spectra are often used in many investigations for materials characterization (in particular for short order and very diluted and dispersed species). A very good overview of 1s XANES spectra of 3d transition metal systems is presented in articles by de Groot.[13,14]

Symmetry of the Metal Site. Regarding the quadrupole and/or dipole nature, the feature at the preedge region of the transition metal 1s edges can be directly related to the symmetry of the metal atoms. The intensity of the preedge peaks is much larger for compounds in which the metal site has tetrahedral symmetry than for (distorted) octahedral systems. This is clearly explained by de Groot as follows:[13] the preedge region is related to transitions to the 3d bands. Both direct 1s → 3d quadrupole transitions and dipole transitions to 4p character hybridized with the 3d band are possible. For the quadrupole transitions, the matrix elements are only about 1% of the dipole transition, but on the other hand, the amount of 3d character is by far larger than the p character. In tetrahedral systems, the local mixing of p and d nature is symmetry allowed, while for a system with inversion symmetry such as octahedral symmetry, it is "forbidden". This rule is relaxed in the solid, and if the density of states is calculated, one finds a small admixture of p states into the 3d band. This admixture is less than for tetrahedral systems, which explains the small preedge. If an octahedral metal site is distorted then, depending on the particular distortion, more p

10.1021/jp049241+ CCC: $27.50
Published on Web 11/26/2004

character will be mixed into the 3d band. The result is that a distortion of the octahedron will show up as an increased intensity of the preedge peaks.

Oxidation State. The higher the oxidation state of the metal, the more positive the overall charge of the atom, and more energy is required to excite an electron out of an orbital.[15] The first formally allowed electric dipole transition is the 1s → 4p transition. Due to the size of the 4p orbital, it overlaps with p orbitals of the ligands, either through σ- or π-bonding. Consequently, this transition is sensitive to the oxidation state and the ligand environment of the metal. For certain symmetries around the metal, the formally electric-dipole forbidden 1s → 3d transition can be observed, which occurs at a lower energy than the main edge transitions.[16] As discussed in the previous paragraph, this transition gains intensity due to the mixing of metal 3d and 4p orbitals, and gives information about the ligand as well as about the oxidation state and symmetry of the metal complex.[17,18]

In this paper we present a XANES study of the K-edges in Cr-, Mn-, Fe-, and Co-oxo species anchored into MCM-41 mesoporous materials via an organometallic precursor. These species were previously characterized by FTIR and Si and Xe NMR in order to determine the nature of the dispersion and location of metal-carbonyl species and their interaction with silanol groups.[12,19] Now, XANES spectra are used as a fingerprint method to determine the nature of the species located inside the MCM-41, or to rule out the presence of specific compounds such as the organometallic precursor or metal oxide species (with Cr, Mn, Fe, or Co). Thermal treatments were performed in all cases to decompose the metal-carbonyl species to the oxides. The observed differences and comparisons with standard compounds allow us to determine important aspects related to the nature of metallic species in MCM-41 channels, such as structure and average oxidation state.

Experimental Section

Sample Preparation. Siliceous MCM-41 samples were prepared using tetraethylorthosilicate (TEOS from Aldrich, 98%), cetyltrimethylammonium bromide (CTAB from Aldrich), deionized water, and ammonia (28%). These silica templated structures were prepared at room temperature using an aqueous solution (i.e., deionized water) of CTAB, TEOS, and NH_4OH for controlling the acidity at pH around 11.5. The synthesis was carried out with CTAB concentration corresponding to molar ratios of 1.0 CTAB:3.7 TEOS:19 NH_4OH:230 H_2O. The main surfactant (CTAB) was mixed with deionized water at 40 °C, then NH_4OH was added dropwise under vigorous stirring during 2 h, while keeping the temperature at 30 °C before addition of TEOS. Then, filtering and washing were followed repeatedly using deionized water; afterward, drying under vacuum at room temperature was performed. The rest of the surfactant was extracted using the Soxhlet system and was calcined in flowing air, using a furnace at 550 °C for 7 h.

The anchoring of $Cr(CO)_6$, $Mn_2(CO)_{10}$, and $Co_2(CO)_8$ species was carried out by means of ultraviolet irradiation ($\lambda = 254$ nm) as follows: 200 mg of MCM-41 was suspended in 30 mL of diethyl ether. Then, $Cr(CO)_6$, $Mn_2(CO)_{10}$, or $Co_2(CO)_8$ (40 mg) was incorporated into the system. This mixture was UV-irradiated at room temperature for 1 h. The obtained sample was transferred to a Schlenk tube and was treated in an ultrasound bath for 15 min at 30 °C, then filtered and washed with anhydrous diethyl ether. On the other hand, the solid containing $Fe_2(CO)_9$ was synthesized using 40 mg of the iron-carbonyl compound, which was added to a suspension of MCM-41 (200 mg) in the Shlenk tube. Then, it was treated in an ultrasound bath for 30 min at 30 °C, followed with filtering and washing with anhydrous diethyl ether.

XANES. The X-ray absorption spectra were measured at the X19A beamline of the NSLS, National Synchrotron Light Source, Brookhaven National Laboratory, Upton, New York, and at the XAS beamline of the LNLS, Laboratorio Nacional do Luz Síncrotron, Campinas, São Paulo, Brazil. XANES spectra at the Cr, Mn, Fe, and Co K-edge (5989, 6539, 7112, and 7709 eV, respectively) were recorded in air at room temperature in transmission mode with two ion chambers as detectors: one before the sample to measure the incident X-ray intensity, I_0, one after the sample and before the corresponding reference metal foil to measure the intensity after the sample, I_1, and one after the metal foil, I_2. The sample and the metal foil spectra were expressed as $\log(I_0/I_1)$ and $\log(I_1/_2)$, respectively. The corresponding spectrum from the metal foil was used to calibrate the absolute energy scale for the corresponding sample spectrum, by positioning the absorption edge at the first inflection point. Monochromators on the beamlines were equipped with Si(111) crystals. The 0.3 mm vertical aperture of the beam definition slit in the hutch provided a resolution of about 2.5 eV at the K absorption edge of the Cr, Mn, Fe, and Co atoms.

Data Reduction. X-ray absorption data were analyzed using standard procedures:[20] a linear background was fit to the preedge region and then subtracted from the entire spectrum, and the jump of the spectrum was normalized to unity with the postedge asymptotic value. To obtain the mean oxidation state of the metal in each sample, the edge shift relative to the metal reference compound was determined following the method proposed by Capehart et al.[21] This method is based on the integration of the normalized absorption spectra for an interval extending from well below the edge up to the first value of energy for which the normalized absorption of the reference is equal to one (E_R). Thus, the integrated absorption of the sample is obtained by integrating up to the energy E_S, whose value is such that the integrated area of the sample and reference absorption are equal (the white line contribution to the normalized absorption area was eliminated taking 80% of the integrated absorption area of the reference). Therefore, the edge shift in the XANES spectrum is given by $\Delta E = E_S - E_R$.

This method is independent of the fine structure, namely, the occurrence of certain peaks or shoulders in the raising edge, contrary to what happens with the simple determination of the inflection points.

The position of the edge is related to the oxidation state of the elements in such a way that the edge energy shifts vary monotonically with the valence of the metal atom.[22] In a set of chemically similar compounds, a linear relationship has been shown between the energy shift and the oxidation state.[22−27] This is true in a model where the energy shift of the core level is mainly due to Coulombic effects.[28,29] Therefore, we performed a linear fit of the oxidation state as a function of the energy shift of different standard bulk oxide compounds corresponding to the same element, and these fits were used to find out the mean oxidation state for metallic-oxo species anchored in the MCM-41, from the edge energy shift determined using Capehart's method.

XANES Results and Discussion

Cr−MCM-41. To interpret the XANES spectra of the sample we measured three Cr reference compounds. Figure 1 shows the normalized XANES spectra of these compounds. Figure 1a corresponds to $Cr(CO)_6$, Figure 1b to Cr_2O_3, and Figure 1c to

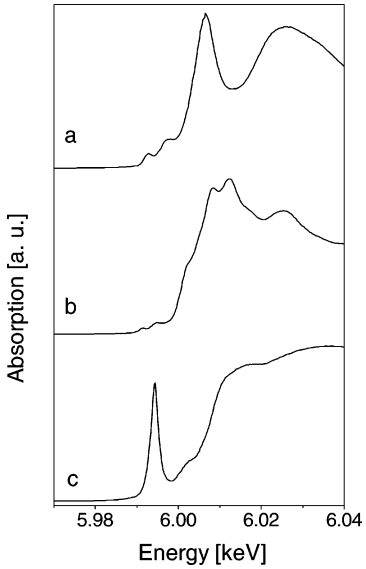

Figure 1. XANES spectra of (a) $Cr(CO)_6$, (b) Cr_2O_3, and (c) $K_2Cr_2O_7$.

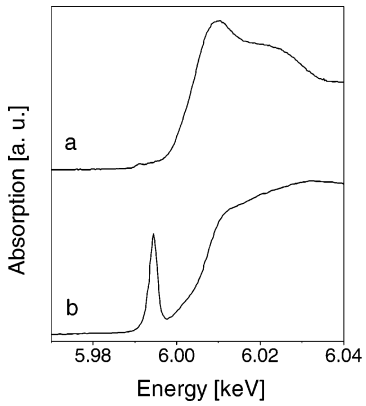

Figure 2. XANES spectra of (a) Cr−MCM-41 and (b) Cr−MCM-41 after oxidation at 400 °C for 2 h.

$K_2Cr_2O_7$. Cr in Cr_2O_3 has octahedral coordination, while in $K_2Cr_2O_7$ it has tetrahedral coordination. A pre-peak is observed for this latter compound at 5994 eV. It is known that this preedge peak for the first-row transition metal ions is originated by a 1s → 3d transition, which is dipole-forbidden in an octahedral compound with an inversion center as seen in the Cr_2O_3 spectrum.[23,30] The spectrum of the carbonyl has a very particular structure and can be easily differentiated from the other reference compounds. Similar to Cr_2O_3, the Cr cation is octahedrally coordinated in the carbonyl species $Cr(CO)_6$, which is consistent with the absence of the preedge peak. This way, the preedge peak region and the characteristics of the spectrum could be used to identify the structure of Cr in the mesoporous material MCM-41.

The energy shifts found for Cr_2O_3 and $K_2Cr_2O_7$ are 11.2 and 18.6 eV, respectively. These values are similar to those reported previously.[24] From these values, the oxidation state of Cr in MCM-41 can also be determined empirically from the XANES spectra.

Figure 2 shows the spectra of Cr−MCM-41 as prepared and after heating in oxygen for 2 h at 400 °C. It is clearly seen that a change in the coordination is produced after the oxidation treatment. The XANES spectrum of Cr−MCM-41 after preparation does not show the preedge peak, and the shape of the edge is very different from that of the carbonyl. This may indicate, at least, that Cr is not in a pure carbonyl form in the MCM-41. The absence of the preedge peak shows that Cr is in

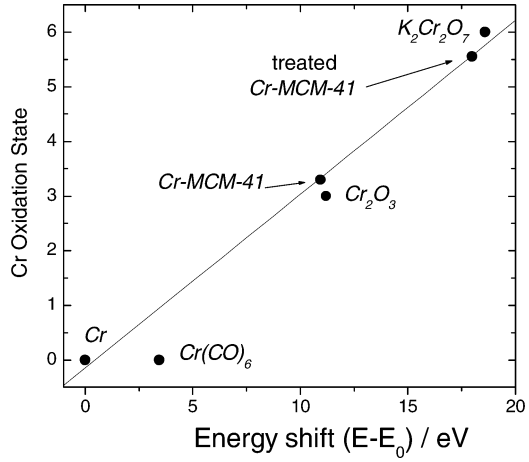

Figure 3. Oxidation state determination of Cr−MCM-41 samples employing a linear fit of the Cr K-edge energy shift of Cr-oxo compounds.

octahedral coordination as in Cr_2O_3. In addition, the XANES profile of Cr−MCM-41 before the thermal treatment is similar to that of Cr_2O_3; however, it is less structured in comparison. This variation can be understood in terms of a slight distortion of the coordination polyhedron of the Cr species anchored to the siloxane surface groups of MCM-41. This fact causes orthogonal symmetry and Cr−O distances to vary slightly from one site to another. The statistical effect in the bulk softens XANES profiles, while the general shape remains.

After the oxidation treatment a strong preedge peak appears at 5994 eV, the same position as that of $K_2Cr_2O_7$. This clearly indicates that after the oxidation the coordination of Cr is tetrahedral. The energy shift of the edge in the as-prepared sample is 16.3 eV, almost the same as that found for Cr_2O_3 so Cr is in a $+3-X$ ($X \ll 1$) valence state. After the oxidation treatment the edge shift is 10.9 eV (see Figure 3). This shows that the exposure to oxygen at 400 °C changes the coordination of Cr from pseudo-octahedral to tetrahedral and Cr is oxidized from a $+3-X$ ($X \ll 1$) to a $+6$ valence state (Figure 3). Thus, before reaction with oxygen at high temperature, our XANES results indicate that the less stable and octahedrally coordinated Cr^{3+}-X species are interacting with silanol groups of the surface of MCM-41, in agreement with the previous FTIR studies.[12,19]

At first, it should not be valid to interpolate predictions about the metal oxidation state for a set of *chemically nonsimilar compounds.* Nevertheless, we incorporated the edge energy shift for metal carbonyl species for completeness for all the elements studied (Cr, Mn, Fe, and Co) in the corresponding figures but we did not use them for the linear fit as, in all cases, their values are far apart from the linear behavior showed for the corresponding metal oxides. This is not surprising since the nature of the ligand environment for metal carbonyls (see for example the work of Schulze et al.[31]) differs considerably from the corresponding chemical environment for metal oxides.

Mn−MCM-41. Figure 4 shows the normalized Mn K-XANES spectra of Mn reference compounds. A single pre-edge peak around 6542 eV in the XANES spectra indicates that Mn atoms occupy sites without a center of inversion. This is more evident for MnO_2 (Figure 4d). However, the intensity of the peak in XANES spectra of the Mn−MCM-41 sample is much lower than that in systems with a regular $[MnO_4]$ species where Mn atoms are tetrahedrally coordinated.[30] This indicates that the coordination geometry of Mn atoms in the samples is at least distorted. Considering the XANES experimental evidence as a fingerprint identification method, at Mn sites in

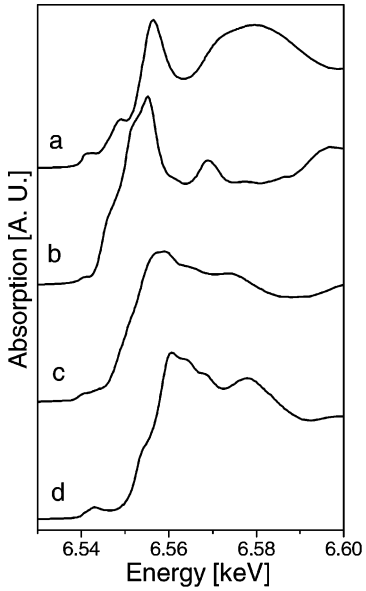

Figure 4. XANES spectra of (a) $Mn_2(CO)_{10}$, (b) MnO, (c) Mn_2O_3, and (d) MnO_2.

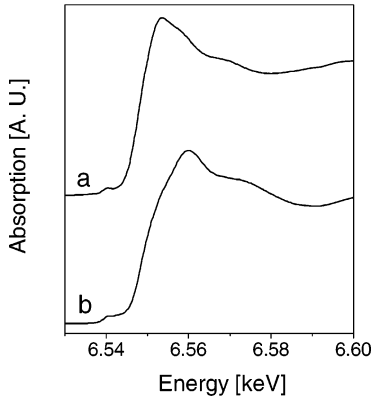

Figure 5. XANES spectra of (a) Mn−MCM-41 and (b) Mn−MCM-41 after oxidation at 400 °C for 2 h.

MCM-41 (before any thermal treatment at high temperature, Figure 5a) the Mn is not forming Mn-carbonyl or Mn-oxide species. After the calcination treatment (Figure 5b) the Mn site symmetry changes noticeably, becoming very close to that in the Mn_2O_3 oxide compound. This fact, as in the previous case with Cr−MCM-41 samples, is indicative of the thermal stability of sub-carbonyl Mn species anchored in the walls of the pores, in agreement again with previous FTIR and NMR results.[12,19] In addition, our interpretation about the tetrahedrally coordinated Mn-oxo species, which seem to be anchored into the MCM-41 porous structure, and which differs from the carbonyls is entirely compatible with recent EXAFS studies performed by Glesson et al.[32,33]

The average oxidation state of the Mn−MCM-41 samples was determined from the linear fit of Figure 6. The magnitude of this shift is comparable to experimental energy shifts in the preedge peak and previously reported Mn K preedge shifts.[34] The present analysis indicates that the formal oxidation state of Mn atoms in the Mn−MCM-41 sample before the oxidation treatment is 2.2, while the same element increases its mean oxidation state value up to 2.9 after the treatment in oxygen at 400 °C for 2 h.

Fe−MCM-41. According to the discussion presented in the Introduction, we would expect that iron compounds with tetrahedral coordination will show a more intense preedge peak

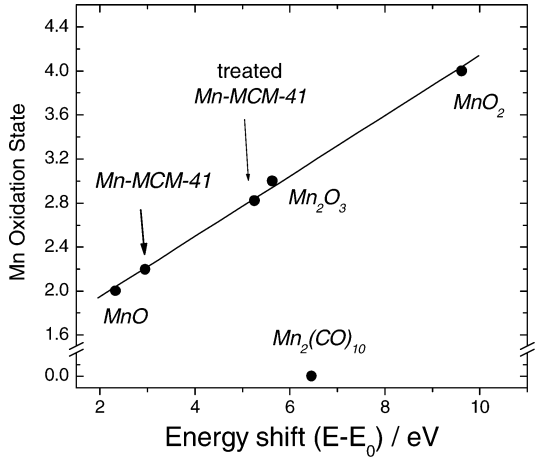

Figure 6. Oxidation state determination of Mn−MCM-41 samples employing a linear fit of the Mn K-edge energy shift of Mn-oxo compounds. The corresponding energy shift for the pure metallic Mn foil was taken as reference (zero of energy shifted for zero oxidation state).

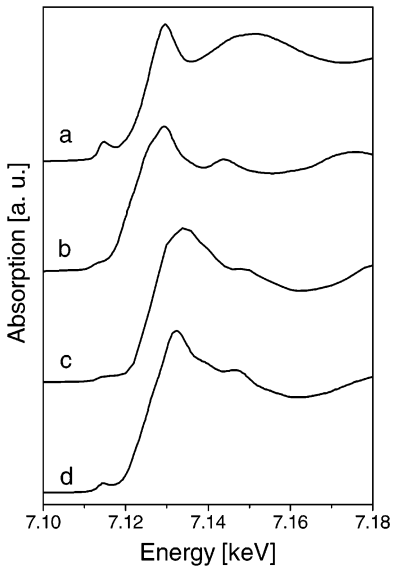

Figure 7. XANES spectra of (a) $Fe_2(CO)_9$, (b) FeO, (c) α-Fe_2O_3, and (d) Fe_3O_4.

than those with octahedral coordination. In this vein we can observe how distorted is the Fe environment in Fe-carbonyl species $Fe_2(CO)_9$ through its very intense prepeak located at 7117 eV (Figure 7a). Several weak preedge peaks are clearly observed in the α-Fe_2O_3 XANES spectrum (Figure 7c). The first two preedge peaks, located at 7113.4 and 7114.8 eV, are assigned to the electronic transitions from the Fe 1s orbital to the crystal-field split t_{2g} and e_g orbitals, respectively.[35] The absorption peaks at the preedge region result from a decrease of local symmetry on the X-ray absorbing atom, and thus the peak intensity can inform on the relative distribution of the T_d sites throughout the compound.

Figure 8 shows the Fe K-edge XANES spectra of Fe−MCM-41 before and after oxidation at 400 °C for 2 h. From comparison with standards compounds (Figure 7) the absence of Fe-carbonyl species is evident. Moreover, the nature of the Fe sites remains unchanged after the treatment. The presence of a prepeak below 7120 eV denotes the existence of Fe in the T_d environment. XANES results do not allow to distinguish the nature of the Fe sites with more detailed information, i.e., the presence of sub-carbonyl species or Fe-oxides species cannot be clearly discriminated from each other.

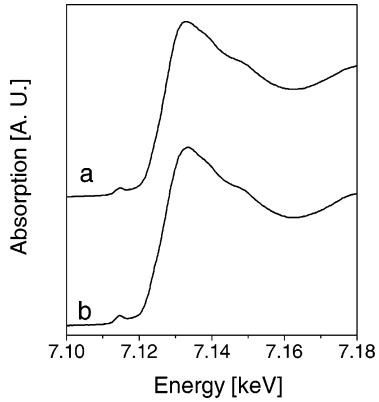

Figure 8. XANES spectra of (a) Fe−MCM-41 and (b) Fe−MCM-41 after oxidation at 400 °C for 2 h.

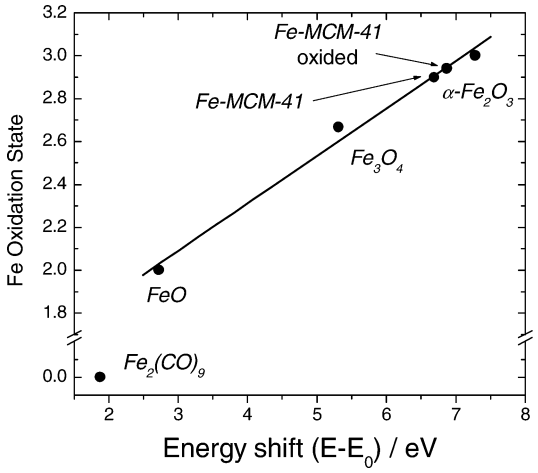

Figure 9. Oxidation state determination of Fe−MCM-41 employing a linear fit of the Fe K-edge energy shift of Fe-oxo compounds. The corresponding energy shift for the pure metallic Fe foil was taken as reference (zero of energy shifted for zero oxidation state).

α-Fe_2O_3 is thermodynamically stable, with all Fe atoms as Fe(III) having rhombohedral structure (Figure 7c) while Fe_3O_4 results in a thermodynamically stable form of Fe(III) and Fe(II) oxide, and FeO has all Fe atoms with a +2 oxidation state. Figure 9 shows Fe oxidation state vs experimental Fe K-edge shift position with respect to the Fermi level for model iron oxide compounds and Fe−MCM-41 samples before and after annealing at 400 °C for 2 h. According to the oxidation state obtained for Fe−MCM-41 samples before and after oxidation (2.90 and 2.94 respectively) we can conclude that Fe atoms are present as Fe(III) in both samples.

Co−MCM-41. Figure 10 shows the normalized XANES spectra of three Co compounds used as references (a: $Co_2(CO)_8$, b: CoO, and c: Co_3O_4) and Figure 11 shows those of the Co−MCM-41 catalyst after preparation and after oxidation at 400 °C for 2 h. Co_3O_4 has a direct spinel-type structure, where Co^{2+} and Co^{3+} cations have tetrahedral and octahedral oxygen coordination, respectively. CoO crystallizes in a fcc NaCl-like structure. In that structure, Co^{2+} ions are situated in the center of the octahedrons where they are surrounded by six oxygen atoms. The cobalt carbonyl structure is formed by two Co atoms each of which is surrounded by four CO molecules.

The XANES profile of Co−MCM-41 differs significantly from those of the three reference compounds. In particular, that of the cobalt carbonyl shows a preedge peak at 7712 eV, which is not observed in the Co−MCM-41 profile. As in previous

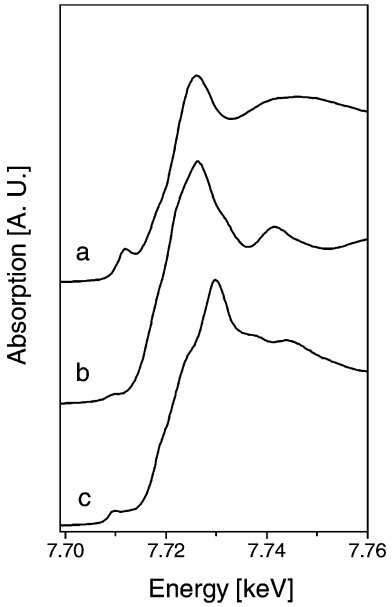

Figure 10. XANES spectra of (a) $Co_2(CO)_8$, (b) CoO, and (c) Co_3O_4.

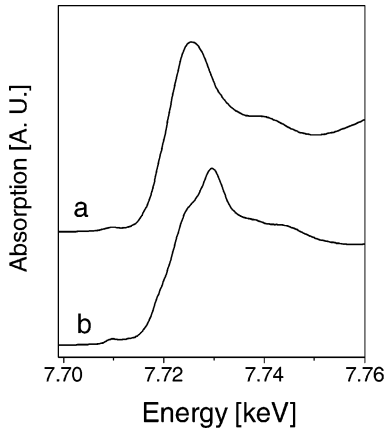

Figure 11. XANES spectra of (a) Co−MCM-41 and (b) Co−MCM-41 after oxidation at 400 °C for 2 h.

cases of Cr and Mn, this suggests that Co is not forming a carbonyl-like structure or a defined oxide structure in the MCM-41. The preedge feature at 7709 is very weak in the Co−MCM-41 profile, and a strong white line is observed. Similar features in the Co XANES profile have been observed for Co−MCM-41 obtained by direct synthesis[36] and for a Co−SBA-15 catalyst reduced at 573 K.[37] After the oxidation treatment at 400 °C the shape of the profile changes and resembles that of the Co_3O_4 oxide, suggesting a total oxidation of the cobalt in the MCM-41 structure. According to this experimental evidence and previous evidence obtained by FTIR and NMR,[12,19] subcarbonyl Co species are interacting with walls of the pores of the MCM-41 at room temperature, and are unstable at higher temperatures such as 400 °C where they form oxides.

Figure 12 shows the relationship between Co oxidation state vs K-edge shift with respect to the Fermi level energy position in the selected series of Co model compounds. The edge positions with respect to the Co metal K-edge at 7709 eV were obtained by area integration of the XANES spectra following the Capehart's method.[21]

It is important to note that for all cases (i.e., Cr, Mn, Fe, and Co) the absence of pure metal carbonyl species cannot be associated with X-ray radiation damage. In effect, it was

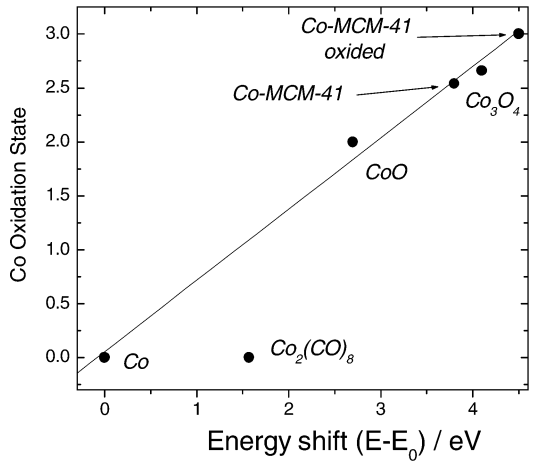

Figure 12. Oxidation state determination of Co−MCM-41 samples employing the Co K-edge energy shift of Co-oxo compounds.

observed previously, not only as isolated species as in our experiments (showed in Figures 1a, 4a, 7a, and 10a for metal carbonyl species of Cr, Mn, Fe, and Co, respectively) but also as anchored in the same type of MCM-41 porous material for Mn,[32,33] in different kinds of ordered porous materials such as Y-zeolite for Mo,[38] and in liquid solution for Tc atoms.[39]

Conclusions

Stable Cr-, Mn-, and Co-oxo species were successfully anchored into the MCM-41 mesoporous walls. By XANES spectroscopy it is possible to perform a detailed analysis of the local environment and average oxidation state of these anchored metal sites. Metal species are not in the same form as their precursors, i.e., metal-carbonyl species. XANES experimental data also clearly indicate that metal atoms are highly dispersed since they are not forming metal oxide bulklike species (an improved determination about coordination shell nature is under analysis using the EXAFS technique on the same samples). Taking this into account, the metal species are probably forming subcarbonyl sub-species covalently bonded to the siloxane groups in the pores of the MCM-41 materials. These systems can be used as a nanometric reactor, which has been found to possess superior catalytic activity during ethylene polymerization reactions as compared to conventional homogeneous carbonyl-based catalysts.[12] The fact that the confined metal species have a different coordination than the carbonyls in solid phase could be the reason for their high catalytic activity. These coordinatively unsaturated surface species would be highly reactive. Additionally, the thermal treatments in O_2 at 400 °C for 2 h apparently decompose the anchored metal sub-carbonyl species. Only for Co−MCM-41 do the oxides formed match the XANES profile corresponding to pure Co_3O_4, while the rest of the metals species are approximately similar to the references used, which leads us to conclude that a further interaction exists with the siloxane groups of the silica pore walls.

Acknowledgment. We acknowledge the partial support of LNLS, Campinas, SP, Brasil (XAS Project No. D04B-XAS1-1192), and Fundación Antorchas (Project No. 14116-120), Argentina, also DGEP (UNAM) and IMP, México. The work carried out by J. A. Rodriguez and J. Y. Kim was financed through contract DE-AC02-98CH10086 with the U.S. Department of Energy (Division of Chemical Sciences). The NSLS is supported by the Divisions of Materials and Chemical Sciences of the U.S. Department of Energy.

References and Notes

(1) Kresge, C. T.; Leonowitz, M. E.; Roth, W. J.; Vartuli, J. C.; Beck, J. S. *Nature* **1992**, *359*, 710−712.

(2) Beck, J. S.; Vartuli, J. C.; Roth, W. J.; Leonowitz, M. E.; Kresge, C. T.; Schmitt, K. D.; Chu, T. W.; Olson, D. H.; Sheppard, E. W.; McCullen, S. B.; Higgins, J. B.; Schlenker, J. L. *J. Am. Chem. Soc.* **1992**, *114*, 10834.

(3) Ying, J. Y.; Mehnert, C. P.; Wong, M. S. *Angew. Chem., Int. Ed.* **1997**, *38*, 556.

(4) Keshavaraja, A.; Ramaswamy, V.; Soni, H. S.; Ramaswamy, A. V.; Ratnasamy, P. *J. Catal.* **1995**, *157*, 501.

(5) Herron, N.; Stucky, C. A. *J. Chem. Soc., Chem. Commun.* **1986**, 1521.

(6) Shevader, S. S.; Raja, R.; Kotasthane, A. N. *Appl. Catal. A* **1999**, *178*, 243.

(7) Hitz, S.; Prins, R. *J. Catal.* **1997**, *168*, 194−206.

(8) Hitz, S.; Kogelbauer, A.; Lindlar, B.; Prins, R. *Stud. Surf. Sci. Catal.* **1998**, *117*, 519.

(9) Abidi, N.; Deroide, A.; Zancheta, J. V.; de Menorval, L. C.; d'Espinose, J. B. *J. Non-Cryst. Solids* **1998**, *231*, 49.

(10) Hammond, W.; Prouzet, E.; Mahanti, S. D.; Pinnavaia, T. J. *Microporous Mesoporous Mater.* **1999**, *27*, 19.

(11) Tanev, P. T.; Pinnavaia, T. J. *Science* **1995**, *267*, 865.

(12) Rosas-Salas, R. Ph.D. Thesis, Universidad Nacional Autónoma de México, 2003.

(13) de Groot, F. M. F. *J. Electron Spectrosc. Relat. Phenom.* **1994**, *1994*, 529.

(14) de Groot, F. M. F. *Chem. Rev.* **2001**, *101*, 1779.

(15) Shulman, R. G.; Yafet, Y.; Eisenberger, P.; Blumberg, W. E. *Proc. Natl. Acad. Sci. U.S.A.* **1976**, *73*, 1384.

(16) Roe, A. L.; Schneider, D. J.; Mayer, R. J.; Pyrz, J. W.; Widom, J.; Que, L., Jr. *J. Am. Chem. Soc.* **1984**, *106*, 1676.

(17) DuBois, J. L.; Mukherjee, P.; Stack, T. D. P.; Hedman, B.; Solomon, E. I.; Hodgson, K. O. *J. Am. Chem. Soc.* **2000**, *122*, 5775.

(18) Westre, T. E.; Kennepohl, P.; DeWitt, J. G.; Hedman, B.; Hodgson, K. O.; Solomon, E. I. *J. Am. Chem. Soc.* **1997**, *119*, 6297.

(19) Rosas-Salas, R.; Domínguez, J. M.; Rachdi, F.; Alvarez, C. *Stud. Surf. Sci. Catal.* **2003**, *146*, 131.

(20) Boon Teo, K. EXAFS: Basic Principles and Data Analysis. *Inorganic Chemistry Concepts*; Jorgensen, C. K., et al., Eds.; Springer: New York, 1986; Vol. 9.

(21) Capehart, T. W.; Herbst, J. F.; Pinkerton, F. E. *Phys. Rev. B* **1995**, *52*, 7907.

(22) Arcon, I.; Mirtic, B.; Kodre, A. *J. Am. Ceram. Soc.* **1998**, *81*, 222.

(23) Wong, J.; Lytle, F. W.; Messmer, R. P.; Maylotte, D. H. *Phys. Rev. B* **1984**, *30*, 5596.

(24) Pak, C.; Haller, G. L. *Microporous Mesoporous Mater.* **2001**, *48*, 165.

(25) Ressler, T.; Wong, J.; Roos, J. *J. Synchrotron Radiat.* **1999**, *6*, 656.

(26) Kataby, G.; Koltypin, Y.; Rothe, J.; Hormes, J.; Felner, I.; Cao, X.; Gedanken, A. *Thin Solid Films* **1998**, *333*, 41.

(27) Fernández-García, M. *Catal. Rev.* **2002**, *44*, 59.

(28) Watson, R. E.; Perlman, M. L.; Herbst, J. F. *Phys. Rev. B* **1976**, *13*, 2358.

(29) Bagus, P. S.; Pacchioni, G.; Sousa, C.; Minerva, T.; Parmigiani, F. *Chem. Phys. Lett.* **1992**, *196*, 641.

(30) Bianconi, A.; Garcia, J.; Benfatto, M.; Marcelli, A.; Natoli, C. R.; Ruiz-Lopez, M. F. *Phys. Rev. B* **1991**, *43*, 6885.

(31) Schulze, I.-K. G.; Handschuh, H.; Ganteför, G.; Eberhardt, W. *Phys. Rev. Lett.* **1996**, *76* (7), 1047.

(32) Burch, R.; Cruise, N. A.; Gleeson, D.; Tsang, S. C. *J. Mater. Chem.* **1998**, *8*, 227.

(33) Gleeson, D.; Burch, R.; Cruise N. A.; Tsang, S. C. *Nanostruct. Mater.* **1999**, *12*, 7.

(34) Manceau, A.; Gorshkov, A. I.; Drits, V. A. *Am. Mineral.* **1992**, *77*, 1133. Manceau, A.; Gorshkov, A. I.; Drits, V. A. *Am. Mineral.* **1992**, *77*, 1144.

(35) Dräger, G.; Frahm, R.; Materlik, G.; Brümmer, O. *Phys. Status Solidi B* **1988**, *146*, 287.

(36) Béland, F.; Badiei, A.; Ronning, M.; Nicholson, D.; Bonneviot, L. *Phys. Chem. Chem. Phys.* **1999**, *1*, 605.

(37) Khodakov, A. Y.; Gribolav-Constant, A.; Bechara, R.; Villain, F. *J. Phys. Chem. B* **2001**, *105*, 9805.

(38) Yamaguchi, A.; Suzuki, A.; Shido, T.; Inada, Y.; Asakura, K.; Nomura, M.; Iwasawa, Y. *J. Phys. Chem B* **2002**, *106*, 2415.

(39) Seifert, S.; Künstler, J.-U.; Gupta, A.; Funke, H.; Reich, T.; Henning, C.; Roβberg, A.; Pietzsch, H.-J.; Alberto, R.; Johansen, B. *Radiochim. Acta* **2000**, *88*, 239.